

A semi-supervised Bayesian approach for simultaneous protein sub-cellular localisation and organelle discovery

Oliver M. Crook^{1,2}, Lisa M. Breckels¹, Daniel J.H. Nightingale¹, Owen Vennard¹, Kathryn S. Lilley¹, Paul D.W. Kirk^{* 2}, and Laurent Gatto^{† 3}

¹ Cambridge Centre for Proteomics, Department of Biochemistry, University of Cambridge, Cambridge, UK

² MRC Biostatistics Unit, Cambridge Institute for Public Health, Cambridge, UK

³ de Duve Institute, UCLouvain, Avenue Hippocrate 75, 1200 Brussels, Belgium

March 17, 2019

Abstract

The cell is compartmentalised into complex micro-environments allowing an array of specialised biological processes to be carried out in synchrony. Determining a protein's sub-cellular localisation to one or more of these compartments can therefore be a first step in determining its function. High-throughput and high-accuracy mass spectrometry based sub-cellular proteomic methods can now shed light on the localisation of thousands of proteins at once. Machine learning algorithms are then typically employed to make protein-organelle assignments. However, these algorithms are limited by insufficient and incomplete annotation. We propose a semi-supervised Bayesian approach to novelty detection, allowing the discovery of additional previously unannotated sub-cellular niches present within the data. Inference in our model is performed in a fully Bayesian framework, allowing us to quantify uncertainty in the allocation of proteins to new sub-cellular niches, as well as in the number of newly discovered compartments. We apply our approach across 10 mass-spectrometry based spatial proteomic datasets, representing a diverse repertoire of experimental protocols. Application of our approach to two *hyperLOPIT* experiments validates its utility by recovering chromatin enrichment preparation without annotation. Novel compartmentalisation is uncovered in experiments on the U 2-OS cell line and this is validated by annotations from the human protein atlas. Moreover, using data from *Saccharomyces cerevisiae*, we uncover a collection of proteins trafficking from the ER to early Golgi.

^{*}paul.kirk@mrc-bsu.cam.ac.uk

[†]laurent.gatto@uclouvain.be

1 Introduction

Aberrant protein sub-cellular localisation has been implicated in numerous diseases, including cancers (Kau *et al.*, 2004), obesity (Siljee *et al.*, 2018), and multiple others (Laurila and Vihinen, 2009). Furthermore, recent estimates suggest that up to 50% of proteins reside in multiple locations with potentially different functions in each localisation (Christoforou *et al.*, 2016; Thul *et al.*, 2017). Characterising the sub-cellular localisation of proteins is therefore of critical importance in order to understand the pathobiological mechanisms and aetiology of many diseases. Proteins are compartmentalised into sub-cellular niches, including organelles, sub-cellular structures, liquid phase droplets and protein complexes. These compartments ensure the biochemical conditions for proteins to function correctly are met, and that they are in the proximity of intended interaction partners (Gibson, 2009). High-throughput and high-accuracy mass-spectrometry (MS) based methods to map the global sub-cellular landscape now exist (Christoforou *et al.*, 2016; Mulvey *et al.*, 2017; Geladaki *et al.*, 2019; Orre *et al.*, 2019). These methods begin with gentle cell lysis, proceeded by sub-cellular fractionation and MS-based proteomics profiling. These spatial proteomics approaches rely on rigorous data analysis and interpretation (Gatto *et al.*, 2010, 2014a).

Current computational approaches in MS-based spatial proteomics rely on machine learning algorithms to make protein-organelle assignments, see (Gatto *et al.*, 2014a) for an overview. If a dataset is insufficiently annotated such that sub-cellular niches that are present in the experimental data are missing from the training dataset then this leads to the classifier making erroneous assignments, resulting in inflated *false discovery rate* (FDR) and uncertainty estimates (where available). Therefore, novelty detection, the process of identifying differences between testing and training data, and organelle discovery is of vital importance in spatial proteomics.

Novelty detection can also prove useful in validating experimental design, either by demonstrating contaminants have been removed or by increasing resolution of organelle classes. Furthermore, organisms for which we have little *a priori* knowledge of their proteome organisation can be challenging to annotate and novelty detection can provide putative evidence for sufficient resolution. Since resolution is an important factor in deciding how the proteome should be annotated, Gatto *et al.* (2018) proposed a quantitative measure of organelle resolution to guide users.

Breckels *et al.* (2013) presented a phenotype discovery algorithm called *phenoDisco* to detect novel sub-cellular niches and alleviate the issue of undiscovered phenotypes. The algorithm uses an iterative procedure and the *Bayesian Information Criterion* (BIC) (Schwarz *et al.*, 1978) is employed to determine the number of newly detected phenotypes. Afterwards the dataset can be re-annotated and a classifier employed to assign proteins to organelles, including those that have been newly detected. Breckels *et al.* (2013) applied their method on several datasets and discovered new organelle classes in *Arabidopsis* (Dunkley *et al.*, 2006) and *Drosophila* (Tan *et al.*, 2009). The approach later successfully identified the trans-Golgi network (TGN) in *Arabidopsis* roots (Groen *et al.*, 2014).

Recently, Crook *et al.* (2018) demonstrated the importance of uncertainty quantification in spatial proteomics. They proposed a generative classification model and took a fully Bayesian approach to spatial proteomics data analysis by computing probability distributions of protein-organelle assignments using Markov-chain Monte-Carlo (MCMC). These

probabilities were then used as the basis of organelle allocations, as well as to quantify the uncertainty in these allocations. On the basis that some proteins cannot be well described by any of the annotated sub-cellular niches, a multivariate student's T distribution was included for outlier detection. The proposed T-Augmented Gaussian Mixture (TAGM) model was shown to achieve state-of-the-art predictive performance against other commonly used machine learning algorithms ([Crook *et al.*, 2018](#)).

Here, we propose an extension to TAGM to allow simultaneous protein-organelle assignments and novelty detection. One assumption of the existing TAGM model is that the number of organelle classes is known. Here, we design a novelty detection algorithm based on allowing an unknown number of additional organelle classes, as well as quantifying uncertainty in this number.

Quantifying uncertainty in the number of components in a Bayesian mixture model is challenging and many approaches have been proposed in the literature (see for example [Ferguson \(1974\)](#); [Antoniak \(1974\)](#); [Richardson and Green \(1997\)](#) and the appendix for further details). Here, we make use of recent asymptotic results in Bayesian analysis of mixture models ([Rousseau and Mengersen, 2011](#)). The principle of overfitted mixtures allows us to specify a (possibly large) maximum number of components. As shown in [Rousseau and Mengersen \(2011\)](#) these components empty if they are not supported by the data, allowing the number of components to be inferred. [Kirk *et al.* \(2012\)](#) previously made use of this approach in the Bayesian integrative modelling of multiple genomic datasets. In our application, some of the organelles may be annotated with known marker proteins and this places a lower bound on the number of sub-cellular niches. Bringing these ideas together results in a semi-supervised Bayesian approach, which we refer to as Novelty TAGM. A schematic overview of the model is displayed in figure 1.

We apply Novelty TAGM to 10 spatial proteomic datasets across a diverse range of protocols, including *hyperLOPIT* ([Christoforou *et al.*, 2016](#); [Mulvey *et al.*, 2017](#)), LOPIT-DC ([Geladaki *et al.*, 2019](#)), dynamic organeller maps ([Itzhak *et al.*, 2016](#)) and spatial-temporal methods ([Beltran *et al.*, 2016](#)). We first validate our approach by recovering chromatin enrichment preparation in *hyperLOPIT* experiments, including mouse pluripotent stem cells and human U 2-OS cells. Application of Novelty TAGM to each dataset reveal additional biologically relevant compartments. Notably, we demonstrate that the U 2-OS *hyperLOPIT* dataset reveals 4 sub-nuclear compartments: the nucleolus, nucleoplasm, chromatin-associated, and the nuclear membrane. These findings are validated using the human protein atlas ([Thul *et al.*, 2017](#); [Sullivan *et al.*, 2018](#)). In addition, an endosomal enriched compartment is robustly identified across *hyperLOPIT* and LOPIT-DC technologies. We also able to uncover small collections of proteins; for example we identify vesicle proteins trafficking from the ER to the early Golgi in a *hyperLOPIT* experiment on *Saccharomyces cerevisiae*.

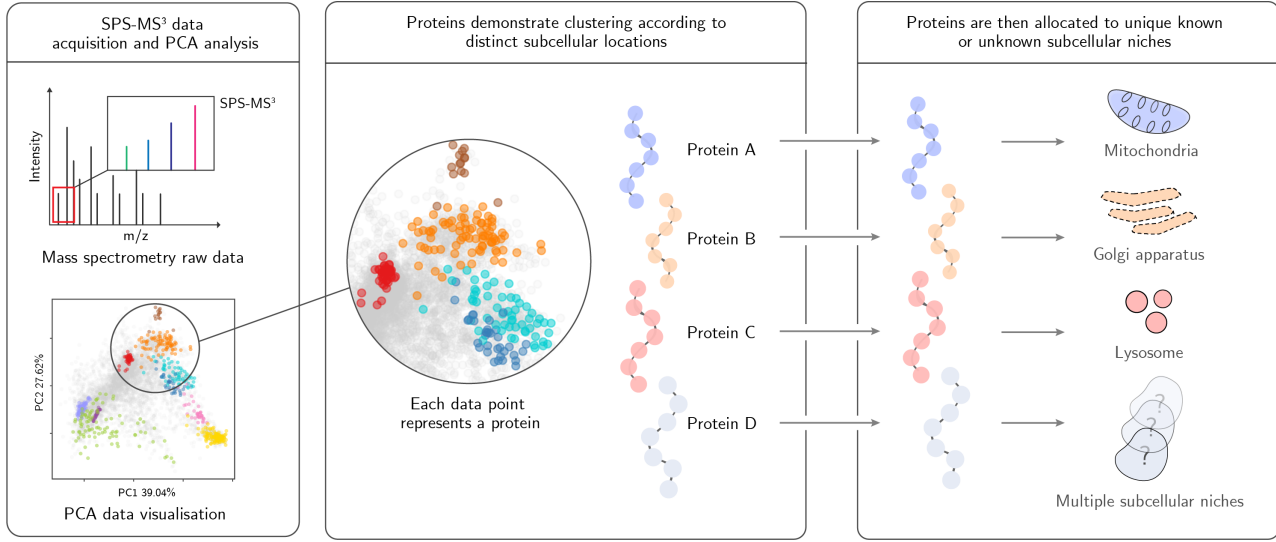


Figure 1: An overview of the Novelty TAGM method.

2 Methods

2.1 Datasets

We provide a brief description of datasets used in this manuscript. We analyse *hyperLOPIT* datasets, in which sub-cellular fractionation is performed using density-gradient centrifugation (Dunkley *et al.*, 2004, 2006; Mulvey *et al.*, 2017), on mouse pluripotent stem cells (Christoforou *et al.*, 2016) and human osteosarcoma (U 2-OS) cells (Thul *et al.*, 2017; Geladaki *et al.*, 2019), as well as a *S. cerevisiae* (bakers’ yeast) dataset (Nightingale *et al.*, 2019). The mouse stem cell dataset combines two 10-plex biological replicates and quantitative information on 5032 proteins. The U 2-OS dataset combines three 20-plex biological replicates and provides information on 4883 proteins. The yeast dataset represents four 10-plex biological replicate experiments performed in *S. cerevisiae* cultured to early-mid exponential phase. This dataset contains quantitative information for 2846 proteins that were common across four 10-plex biological replicate experiments. Tandem Mass Tag (TMT) (Thompson *et al.*, 2003) labelling was used in all *hyperLOPIT* experiments with LC-SPS-MS3 used for high accuracy MS-based quantitation (Ting *et al.*, 2011; McAlister *et al.*, 2014). Beltran *et al.* (2016) integrated a temporal component to the analysis of the LOPIT protocol. They analysed HCMV infected primary fibroblast cells over 5 days, producing a control and infected map every 24 hours. We analyse the control and infected map 24 hours post infection, providing information on 2220 and 2196 proteins respectively. In a comparison with *phenoDisco*, we apply Novelty TAGM to HEK-293 cells that were analyses using the LOPIT protocol, using iTRAQ 8-plex quantifying 1371 proteins (Breckels *et al.*, 2013).

Our approach is not limited to spatial proteomics data where the sub-cellular fractionation is performed using density gradients. We demonstrate this through the analysis of the dynamic organeller maps (DOM) protocols (Itzhak *et al.*, 2016, 2017), which quantify 3766 and 8985 proteins respectively. These approaches used label-free quantitation with fractionation performed using differential centrifugation. We analyse 6 replicates from the

HeLa cell line analyses in Itzhak *et al.* (2016) and 3 replicates of mouse primary neurons from Itzhak *et al.* (2017). Hirst *et al.* (2018) also used the DOM protocol and coupled CRISPR-CAS9 knockouts with spatial proteomics designed to explore the functional role of AP-5. We analyse the control map from this experiment. Finally, we consider the U 2-OS data using the LOPIT-DC protocol (Geladaki *et al.*, 2019), which quantified 6837 across 3 biological replicates. Though we do not consider a PCP based spatial proteomics datasets in this manuscript, our method also applies to such data (Foster *et al.*, 2006; Kristensen *et al.*, 2012; Kristensen and Foster, 2014).

2.2 Model

2.2.1 Spatial proteomics mixture model

In this section, we briefly review the TAGM model proposed by (Crook *et al.*, 2018). Let N denote the number of observed protein profiles each of length L , corresponding to the number of quantified fractions. The quantitative profile for the i -th protein is denoted by $\mathbf{x}_i = [x_{1i}, \dots, x_{Li}]$. In the original formulation of the model it is supposed that there are K known sub-cellular compartments to which each protein could localise (e.g. cytoplasm, endoplasmic reticulum, mitochondria, \dots). For simplicity of exposition, we refer to these K sub-cellular compartments as *components*, and introduce component labels z_i , so that $z_i = k$ if the i -th protein localises to the k -th component. To fix notation, we denote by X_L the set of proteins whose component labels are known, and by X_U the set of unlabelled proteins. If protein i is in X_U , we want the probability that $z_i = k$ for each $k = 1, \dots, K$; that is, for each unlabelled protein, the probability of belonging to each component (given a model and the observed data).

The distribution of quantitative profiles associated with each protein that localise to the k -th component is modelled as multivariate normal with mean vector $\boldsymbol{\mu}_k$ and covariance matrix Σ_k . However, many proteins are dispersed and do not fit this assumption. To model these "outliers" Crook *et al.* (2018) introduced a further indicator variable ϕ . Each protein \mathbf{x}_i is then described by an additional variable ϕ_i , with $\phi_i = 1$ indicating that protein \mathbf{x}_i belongs to an organelle derived component and $\phi_i = 0$ indicating that protein \mathbf{x}_i is not well described by these known components. This outlier component is then modelled as a multivariate T distribution with degrees of freedom κ , mean vector \mathbf{M} , and scale matrix V . Thus the model can be written as:

$$\mathbf{x}_i | z_i = k, \phi_i \sim \mathcal{N}(\boldsymbol{\mu}_k, \Sigma_k)^{\phi_i} \mathcal{T}(\kappa, \mathbf{M}, V)^{1-\phi_i}. \quad (1)$$

Let $f(\mathbf{x}|\boldsymbol{\mu}, \Sigma)$ denote the density of the multivariate normal with mean vector $\boldsymbol{\mu}$ and covariance matrix Σ evaluated at \mathbf{x} and $g(\mathbf{x}|\kappa, \mathbf{M}, \mathbf{V})$ denote the density of the multivariate T-distribution. For any i , the prior probability of the i -th protein localising to the k -th component is denoted by $p(z_i = k) = \pi_k$. Letting $\boldsymbol{\theta} = \{\boldsymbol{\mu}_k, \Sigma_k\}_{k=1}^K$ denote the set of all component mean and covariance parameters, and $\boldsymbol{\pi} = \{\pi_k\}_{k=1}^K$ denote the set of all mixture weights, it follows that:

$$p(\mathbf{x}_i|\boldsymbol{\theta}, \boldsymbol{\pi}, \phi_i, \kappa, \mathbf{M}, V) = \sum_{k=1}^K \pi_k (f(\mathbf{x}_i|\boldsymbol{\mu}_k, \Sigma_k)^{\phi_i} g(\mathbf{x}_i|\kappa, \mathbf{M}, V)^{1-\phi_i}). \quad (2)$$

For any i , we set the prior probability of the i -th protein belonging to the outlier component as $p(\phi_i = 0) = \epsilon$.

Equation (2) can then be rewritten in the following way:

$$p(\mathbf{x}_i|\boldsymbol{\theta}, \boldsymbol{\pi}, \kappa, \epsilon, \mathbf{M}, V) = \sum_{k=1}^K \pi_k ((1 - \epsilon)(f(\mathbf{x}_i|\boldsymbol{\mu}_k, \Sigma_k) + \epsilon g(\mathbf{x}_i|\kappa, \mathbf{M}, V)), \quad (3)$$

As in [Crook et al. \(2018\)](#), we fix $\kappa = 4$, \mathbf{M} as the global empirical mean, and V as half the global empirical variance of the data, including labelled and unlabelled proteins. To extend this model to permit novelty detection, we specify the maximum number of components $K_{max} > K$. Our proposed model then allows up to $K_{novelty} = K_{max} - K \geq 0$, new phenotypes to be detected. Equation 3 can then be written as

$$\begin{aligned} p(\mathbf{x}_i|\boldsymbol{\theta}, \boldsymbol{\pi}, \kappa, \epsilon, \mathbf{M}, V) &= \sum_{k=1}^K \pi_k ((1 - \epsilon)(f(\mathbf{x}_i|\boldsymbol{\mu}_k, \Sigma_k) + \epsilon g(\mathbf{x}_i|\kappa, \mathbf{M}, V)) \\ &\quad + \sum_{k=K+1}^{K_{max}} \pi_k ((1 - \epsilon)(f(\mathbf{x}_i|\boldsymbol{\mu}_k, \Sigma_k) + \epsilon g(\mathbf{x}_i|\kappa, \mathbf{M}, V)), \end{aligned} \quad (4)$$

where, in the first summation, the K components correspond to known sub-cellular niches and the second summation corresponds to the new phenotypes to be inferred. The parameter sets are then augmented to include these possibly new components; that is, we redefine $\boldsymbol{\theta} = \{\boldsymbol{\mu}_k, \Sigma_k\}_{k=1}^{K_{max}}$ to denote the set of all component mean and covariance parameters, and $\boldsymbol{\pi} = \{\pi_k\}_{k=1}^{K_{max}}$ denote the set of all mixture weights. Relying on the principle of over-fitted mixtures [Rousseau and Mengersen \(2011\)](#), components that are not supported by the data are left empty with no proteins allocated to them. We find setting $K_{novelty} = 10$ is ample to detect new phenotypes.

2.2.2 Bayesian inference and convergence

We perform fully Bayesian inference, using Markov-chain Monte-Carlo methods. We make modifications to the collapsed Gibbs sampler approach used previously in [Crook et al. \(2018\)](#) to allow inference to be performed for the parameters of the novel components (see supplement for full details). Since the number of occupied components at each iteration is random, we can monitor this quantity as a convergence diagnostic. At convergence the number of occupied components is not necessarily fixed, but oscillates around a fixed mode.

2.2.3 Visualising patterns in uncertainty

To simultaneously visualise the uncertainty in the number of newly discovered phenotype, as well as the uncertainty in the allocation of protein to new components we use the so-called

posterior similarity matrix (PSM) (Fritsch and Ickstadt, 2009). The PSM is an $N \times N$ matrix where the $(i, j)^{th}$ entry is the posterior probability that protein i and protein j reside in the same component. Throughout we use a heatmap representation of this quantity. The PSM is summarised into a clustering by maximising the posterior expected adjusted Rand index (see appendix for details)(Fritsch and Ickstadt, 2009). Formulating inference around the PSM also avoids some technical statistical challenges, which are discussed in detail in the appendix.

2.2.4 Uncertainty Quantification

We may be interested in quantifying the uncertainty in whether a protein belongs to a new sub-cellular component. Indeed it is important to distinguish whether a protein belongs to a new phenotype or if we simply have large uncertainty about its localisation. The probability that protein i belongs to a new component is computed from the following equation:

$$P(z_i \in \{K + 1, \dots, K_{max}\} | X) = 1 - P(z_i \in \{1, \dots, K\} | X), \quad (5)$$

$$(6)$$

which we can approximate by the following Monte-Carlo average:

$$1 - \frac{1}{T} \sum_{t=1}^T P(z_i^{(t)} \in \{1, \dots, K\} | X) = 1 - \frac{1}{T} \sum_{t=1}^T \sum_{k=1}^K P(z_i^{(t)} = k | X) \quad (7)$$

Since the summation in equation 7 only goes up to K (the number of annotated organelles), this equation is identifiable. Throughout we refer to this as the discovery probability.

2.3 Validating computational approaches

In a supervised framework the performance of computational methods can be assessed by using the training data, where a proportion of the training data is withheld from the classifier to be used for the assessment of predictive performance. In an unsupervised framework or semi-supervised framework we cannot validate in this way, since there is no ground truth with which to compare. Thus, we propose three approaches, using external information, for independent validation of our method. Table 1 summarises the differences between the current available machine-learning methods for spatial proteomics.

2.3.1 Artificial masking of annotations to recover experimental design

Removing the annotations from an entire component and assessing the ability of our method to rediscover these annotations is one form of validation. We consider this validation approach in several of the datasets; in particular, chromatin enrichment is performed in two of the *hyperLOPIT* experiments, where the intention is to increase the resolution between chromatin and non-chromatin associated nuclear proteins (Mulvey *et al.*, 2017). As validation of our method we hide these annotations and rediscover them in a unbiased fashion.

2.3.2 The human protein atlas

A further approach to validating our method is to use an orthogonal spatial proteomic information. The human protein atlas ([Thul et al., 2017](#); [Sullivan et al., 2018](#)) provides confocal microscopy information on thousands of proteins, using validated antibodies. When we consider a dataset for which there is HPA annotations we use this data to validate the novel phenotypes for biological relevance.

2.3.3 Gene-Ontology term enrichment

The gene ontology provides a database of relationships between genes and classes according to similar functional annotation. One of these annotations is cellular compartment which we exploit in our analysis. Throughout, we perform GO enrichment analysis with FDR control performed according the Benjamini-Hochberg procedure ([Benjamini and Hochberg, 1995](#); [Ashburner et al., 2000](#); [Yu et al., 2012](#)). The proteins in each novel phenotype are assessed in turn for enriched cellular compartment term, against the background of all quantified protein in that experiment.

Method	MS-based Spatial Proteomics Computational Methods							
	Localisation Prediction	Uncertainty in protein localisation	Outlier detection	Novelty detection	Uncertainty in number novel phenotypes	Uncertainty in allocation to new phenotypes	Integrative	
Supervised Machine Learning(Gatto et al., 2014a)	✓	✗	✗	✗	✗	✗	✗	✗
Transfer Learning (Breckels et al., 2016)	✓	✗	✗	✗	✗	✗	✗	✓
<i>PhenoDisco</i> (Breckels et al., 2013)	✗	✗	✓	✓	✗	✗	✗	✗
TAGM (Crook et al., 2018)	✓	✓	✓	✗	✗	✗	✗	✗
Novelty TAGM (This manuscript)	✓	✓	✓	✓	✓	✓	✓	✗

Table 1: Summary of computational methods for spatial proteomics datasets.

3 Results

3.1 Validating experimental design in *hyperLOPIT*

To validate Novelty TAGM, we apply our method to a mouse stem cell *hyperLOPIT* dataset (Christoforou *et al.*, 2016) and a recent human osteosarcoma (U 2-OS) *hyperLOPIT* dataset (Thul *et al.*, 2017; Geladaki *et al.*, 2019). These experimental protocols used a chromatin enrichment step to resolve nuclear chromatin associated proteins from nuclear proteins not associated with the chromatin. Removing the nuclear, chromatin and ribosomal annotations from the datasets, we test the ability of Novelty TAGM to recover them.

3.1.1 Mouse pluripotent embryonic stem cells

For the mouse stem cell dataset, Novelty TAGM reveals 8 new phenotypes, which we refer to as phenotype 1,..., phenotype 8, for which there is at least 1 protein with discovery probability greater than 0.95. Novelty TAGM recovers these hidden annotations with phenotype 2 having the enriched terms associated with chromatin, such as *chromatin* and *chromosome* ($p < 10^{-80}$). Phenotype 3 corresponds to a separate nuclear substructure with enrichment for the terms *nucleolus* ($p < 10^{-60}$) and *nuclear body* ($p < 10^{-30}$). Thus, in the mouse stem cell dataset Novelty TAGM confirms the chromatin enrichment preparation designed to separate chromatin and non-chromatin associated nuclear proteins (Mulvey *et al.*, 2017). In addition, phenotype 4 demonstrates enrichment for the ribosome annotation ($p < 10^{-35}$). Phenotype 1 is enriched for *centrosome* and *microtubule* annotations ($p < 10^{-15}$), though observing the PSM in figure 2 we can see there is much uncertainty in this phenotype. This uncertainty quantification can then be used as a basis for justifying additional expert annotation.

3.1.2 The human osteosarcoma (U 2-OS) cell-line

Now turning to the U 2-OS cancer cell-line dataset, Novelty TAGM reveals 9 new phenotypes for which there is at least 1 protein with a greater discovery probability than 0.95. These phenotypes along with the uncertainty associated with them are visualised in figure 2. We first consider the HPA confocal microscopy data for validation (Thul *et al.*, 2017; Sullivan *et al.*, 2018). The HPA provides information on the same cell-line and therefore constitutes an excellent complementary resource. This *hyperLOPIT* dataset was already shown to be in strong agreement with the microscopy data. Proteins in phenotypes 3,4,5 and 8 have a nuclear related annotation at their most frequent annotation in the HPA data. Then GO enrichment analysis reveals *chromatin* and *chromosome* annotations for phenotype 3 ($p < 10^{-40}$). Phenotype 4 is enriched for the *nucleolus* ($p < 10^{-60}$), furthermore nucleoli and nucleoli/nucleus are the 2nd and 3rd most frequent HPA annotation for proteins belonging to this phenotype. For phenotype 5 the most associated term is nucleoplasm from the HPA data, as well as GO enrichment ($p < 10^{-10}$). Phenotype 8 has the nuclear membrane as its most frequent HPA annotation and this is supported by GO enrichment with the terms nuclear membrane and nuclear envelope associated with proteins in this phenotype ($p < 10^{-10}$). Thus, Novelty TAGM has not only confirmed successful validation of chromatin enrichment, but also demonstrated other sub-nuclear level resolution. In addition, phenotype 1 is enriched for *ribosome* ($p < 10^{-20}$), whilst phenotype 2 is enriched for *endosomes* ($p < 10^{-30}$).

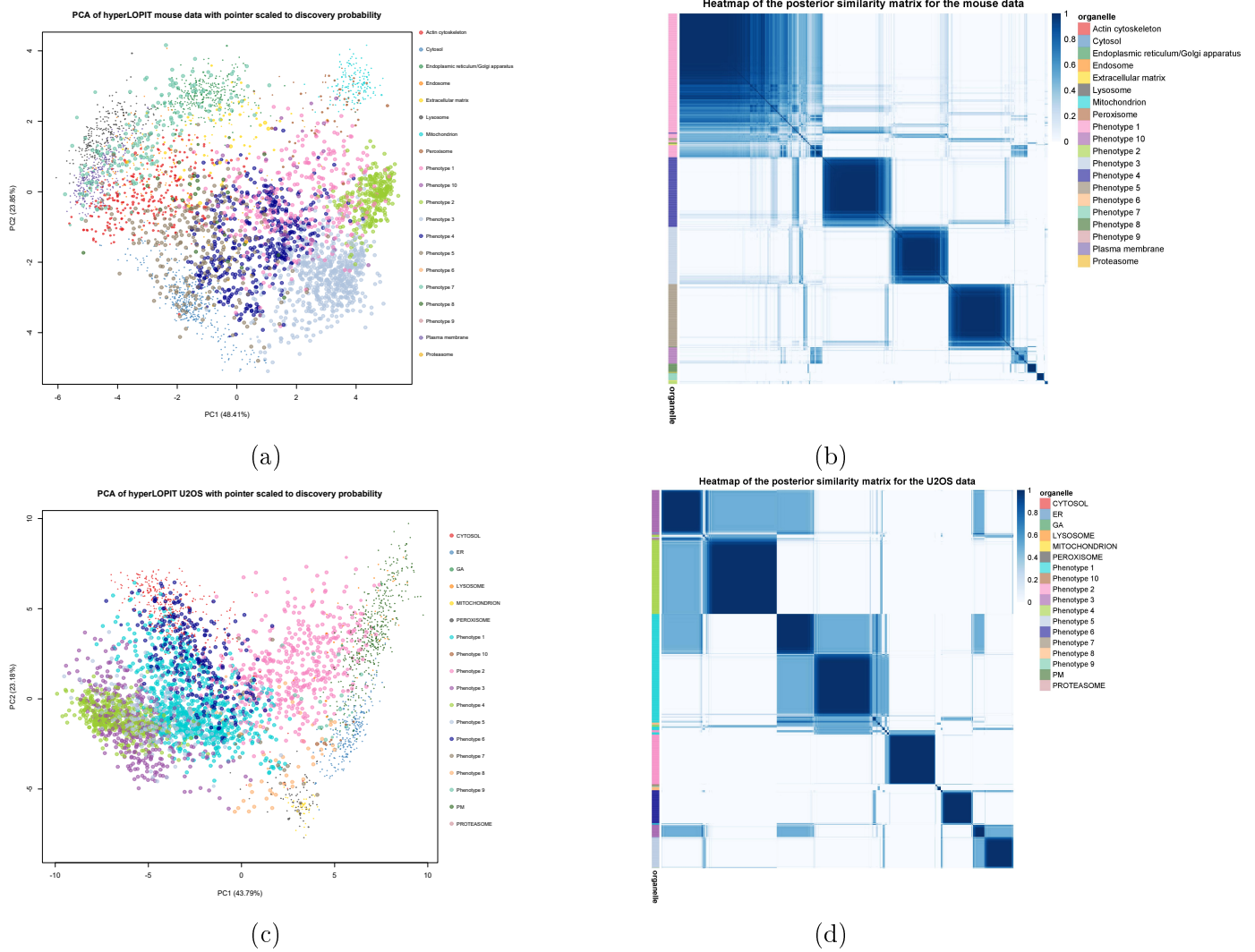


Figure 2: (a,c) PCA plots of the *hyperLOPIT* mouse pluripotent stem cell data and the *hyperLOPIT* U 2-OS cancer cell-line data. The points are coloured according to the organelle or proposed new phenotype and are scaled according to the discovery probability. The PCA plot reveals clear clustering structure in the data and confidently identified new phenotypes. (b,d) Heatmaps of the posterior similarity matrix derived from the mouse stem cell data and the U 2-OS cell line data demonstrating the uncertainty in the clustering structure of the data. We have only plotted the proteins which have greater than 0.99 probability of belonging to a new phenotype and probability of being an outlier less than 0.95 (0.5 for the U 2-OS dataset to reduce the number of visualised proteins.).

3.2 Uncovering additional sub-cellular structures

Having validated the ability of Novelty TAGM to recover known experimental design, as well as uncover additional sub-cellular niches resolved in the data we turn to apply Novelty TAGM to several additional datasets.

3.2.1 U 2-OS cell line revisited

We first consider the LOPIT-DC dataset on the U 2-OS cell line ([Geladaki et al., 2019](#)). For additional validation of our proposed method we removed the nuclear, proteosomal, and ribosomal annotations. Novelty TAGM reveals 10 phenotypes with at least 1 protein with a discovery probability of greater than 0.99 and outlier probability of less than 0.95. These clusters and the uncertainty associated with them can be visualised in figure 3.

In a similar vein to the analysis performed on the *hyperLOPIT* U 2-OS dataset, we initially use the available HPA to validate these clusters ([Thul et al., 2017](#)). Phenotypes 3, 5, 7 and 9 have their most frequent HPA annotation as nuclear associated. To obtain additional functional information about these phenotypes, we perform an over-representation analysis on GO cellular compartment terms. Phenotype 3 reveals both nucleolus ($p < 10^{-60}$) and ribosome ($p < 10^{-30}$) annotations. Phenotype 5 reveals a proteasome cluster ($p < 10^{-30}$). A chromatin enriched phenotype is also discovered, with phenotype 9 having chromosome ($p < 10^{-60}$) and chromatin ($p < 10^{-40}$) terms significantly over-represented in these clusters. The first evidence for sub-nuclear resolution in this LOPIT-DC dataset. Phenotype 6 represents a cluster with mixed annotation with over-representation for both plasma membrane ($p < 10^{-8}$) and the extracellular matrix ($p < 10^{-2}$), this is supported by HPA annotation with vesicles, cytosol, and plasma membrane the top three annotations. An extracellular phenotype was not previously known in these data. Furthermore, phenotype 8 is significantly enriched for endosomes ($p < 10^{-55}$), again a novel annotation for this data. In addition, 107 of the proteins in this phenotype are also localised to the endosome-enriched phenotype presented in the U 2-OS *hyperLOPIT* dataset. Thus, we robustly identify new phenotypes across highly different spatial proteomics protocols. Hence, we have presented strong evidence for additional annotations in this dataset beyond the original analysis of this dataset ([Geladaki et al., 2019](#)); in particular, we have described sub-nuclear resolution with separated chromatin and non-chromatin classes. In addition, we have joint evidence for an endosomal cluster in both the LOPIT-DC and *hyperLOPIT* dataset. Finally, through the discovery probability and by using the PSMs, we have quantified uncertainty in these proposed phenotypes providing rich information for rigorous interrogation of these datasets.

3.2.2 *Saccharomyces cerevisiae*

Novelty TAGM uncovers 8 phenotypes in the yeast *hyperLOPIT* data with at least 1 protein with discovery probability greater than 0.95. 4 of these phenotypes have no significant over-represented annotations. The first phenotype is enriched for the cell periphery ($p < 10^{-19}$) and fungal-type vacuole ($p < 10^{-10}$). Phenotype 3 has over-represented annotations for the kinetochore ($p < 0.01$), whilst phenotype 4 is enriched for the cytoskeleton ($p < 10^{-7}$). Phenotype 8 represent a joint Golgi and ER cluster with the COPII-coated ER to Golgi transport vesicle enriched in this phenotype ($p < 10^{-14}$), along with the endoplasmic

reticulum membrane ($p < 10^{-10}$) and the Golgi membrane ($p < 10^{-9}$). Indeed, most of the proteins in this phenotype have roles in the early secretory pathway that involve either transport from the ER to the early Golgi apparatus, or retrograde transport to the ER (Bue *et al.*, 2006; Inadome *et al.*, 2005; Otte *et al.*, 2001; Yofe *et al.*, 2016), also reviewed in (Delic *et al.*, 2013). The protein Ksh1p is further suggested through homology with higher organisms to be part of the early secretory pathway (Wendler *et al.*, 2010). The proteins Scw4p, Cts1p and Scw10p (Cappellaro *et al.*, 1998), as well as Pst1p (Pardo *et al.*, 2004), and Cwp1p (Yin *et al.*, 2005), however, are annotated in the literature as localising to the cell wall or extracellular region. It is therefore possible that their predicted co-localisation with secretory pathway proteins observed here represents a snapshot of their trafficking through the secretory pathway. The protein Ssp120p is of unknown function and localises in high throughput studies to the vacuole (Yofe *et al.*, 2016) and the cytoplasm in a punctate pattern (Huh *et al.*, 2003). The localisation observed here may suggest that it is therefore either part of the secretory pathway, or traffics through the secretory pathway for secretion or to become a constituent of the cell wall.

3.2.3 HCMV infected fibroblast cells

We apply Novelty TAGM to the HCMV infected fibroblast cells 24 hours post infection (hpi) (Beltran *et al.*, 2016), and discover 9 additional phenotypes with at least 1 protein with discovery probability greater than 0.95 demonstrated in figure 3. Phenotype 2 contains a singleton protein and phenotypes 4, 6, 7, 8 and 9 are not significantly enriched for any annotations. However, phenotype 3 is enriched for the mitochondrial membrane and envelope annotations ($p < 10^{-4}$), this is an addition to the already annotated mitochondrial class indicating sub-mitochondrial resolution. Phenotype 1 is a mixed ribosomal/nuclear cluster with enrichment for nucleoplasm ($p < 10^{-5}$) and the small ribosomal subunit ($p < 10^{-4}$), which is distinct from phenotype 5 which is enriched for the large ribosomal subunit ($p < 10^{-10}$). This demonstrates unbiased separation of the two ribosomal subunits, which was overlooked in the original analysis (Beltran *et al.*, 2016).

3.2.4 Fibroblast cells without infection

Novelty TAGM reveals 7 phenotypes with at least 1 protein with discovery probability greater than 0.95 in the control fibroblast cells. Phenotypes 2, 4, 5, 6 and 9 have no significantly enriched Gene Ontology terms (threshold $p = 0.01$). However, we observe a phenotype with ribosomal enrichment with the large ribosomal subunit enriched in phenotype 3 with significance at level $p < 10^{-7}$. Phenotype 1 represents a mixed peroxisome ($p < 10^{-2}$) and mitochondrion cluster ($p < 10^{-2}$), an unsurprising results since the mitochondrion and peroxisome have similar biochemical fractionation properties. The differing number of confidently identified and biologically relevant phenotypes discovered between the two fibroblast datasets, could be down to the differing levels of structure between the two datasets. From figure 4 we see differing levels of clustering structure in these datasets.

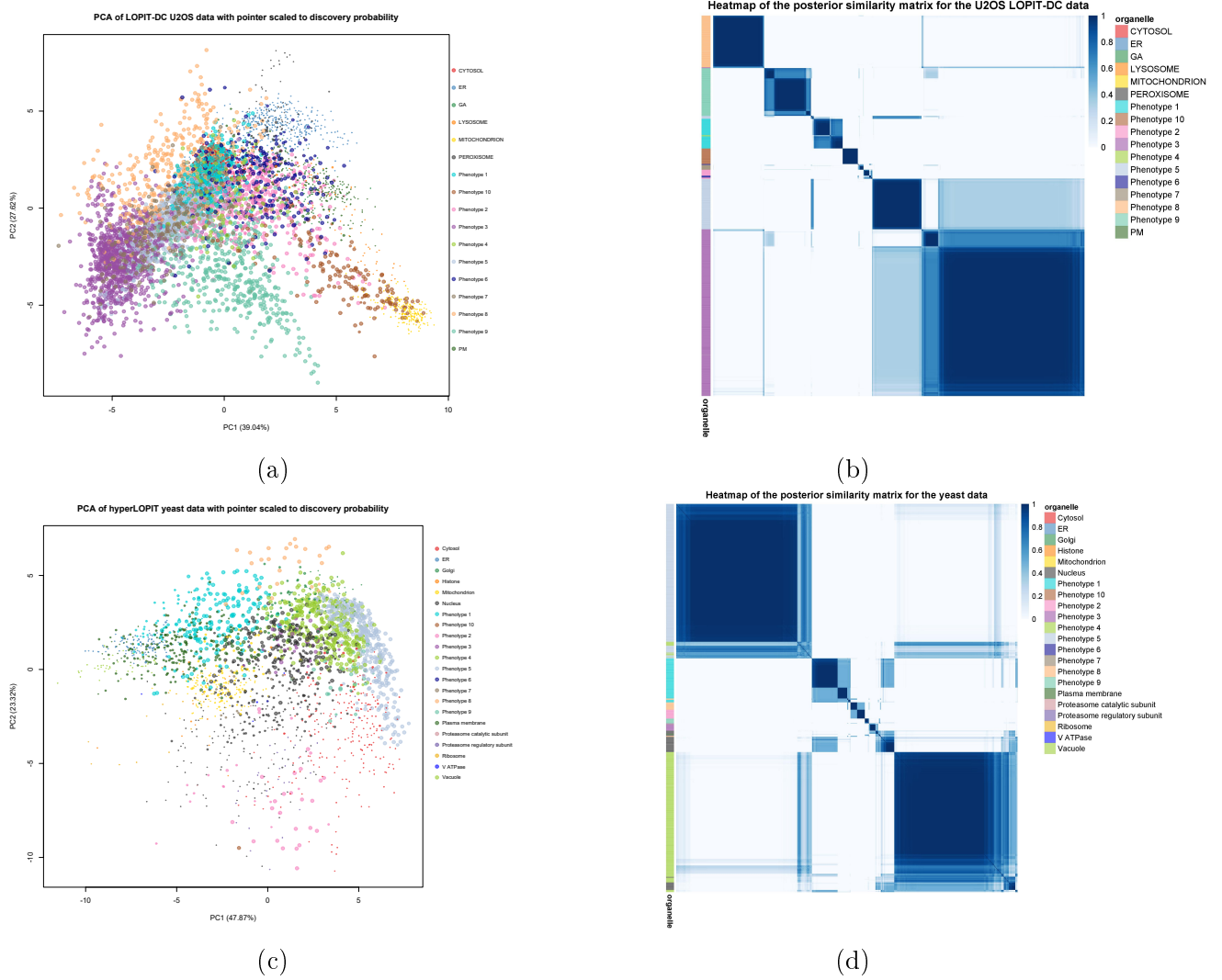


Figure 3: (a, c) PCA plots of the LOPIT-DC U 2-OS data and the *hyper*LOPIT yeast data. The points are coloured according to the organelle or proposed new phenotype and are scaled according to the discovery probability. The PCA plots reveals clear clustering structure in the data and confidently identified new phenotypes. (b,d) Heatmaps of the posterior similarity matrix derived from the U 2-OS dataset and yeast dataset demonstrating the uncertainty in the clustering structure of the data. We have only plotted the proteins which have greater than 0.99 probability of belonging to a new phenotype and probability of being an outlier less than 0.95 (10^{-5} for LOPIT-DC to reduce number of visualised proteins).

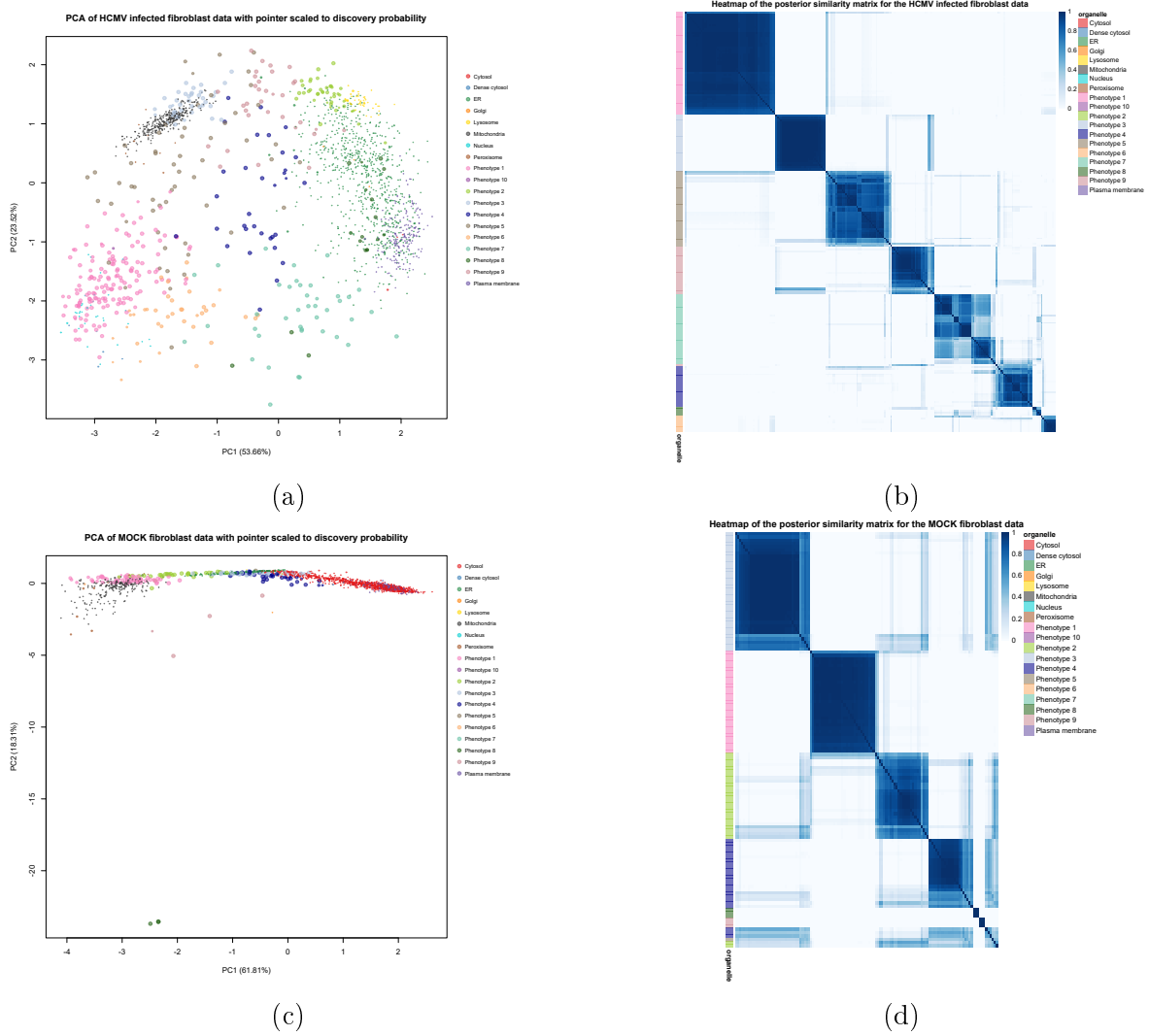


Figure 4: (a, c) PCA plots of the HCMV infected fibroblast data 24 hpi and the mock fibroblast data 24 hpi. The points are coloured according to the organelle or proposed new phenotype and are scaled according to the discovery probability. The PCA plot reveals clear clustering structure in the data and confidently identified new phenotypes. (b, d) Heatmaps of the posterior similarity matrix derived from the infected fibroblast data and mock fibroblast data demonstrating the uncertainty in the clustering structure of the data. We have only plotted the proteins which have greater than 0.99 probability of belonging to a new phenotype and probability of being an outlier less than 0.95.

3.3 Refining annotation in organeller maps

The dynamic organeller map (DOM) protocol was developed to reduce the time taken to perform MS-based spatial proteomic mapping albeit at the cost of organelle resolution (Itzhak *et al.*, 2016; Gatto *et al.*, 2018). The three dataset analysed here are two HeLa cell line (Itzhak *et al.*, 2016; Hirst *et al.*, 2018) and a mouse primary neuron dataset (Itzhak *et al.*, 2017). All three of these datasets have been annotated to contain a mixed class called "Large Protein Complexes". This class contains a mixture of cytosolic, ribosomal, proteosomal and nuclear sub-compartment that pellet during the centrifugation step used to capture this mixed fraction (Itzhak *et al.*, 2016). We apply Novelty TAGM to these data and remove this "Large Protein Complex" annotation, to derive more precise annotations for these datasets.

3.3.1 HeLa cells (Itzhak et. al 2016)

The HeLa dataset of Itzhak *et al.* (2016), which we refer to as HeLa Itzhak, has 3 additional phenotypes uncovered by Novelty TAGM. The first phenotype is enriched for the mitochondrial membrane ($p < 0.01$) distinct from the already annotated mitochondrial class. Phenotype 2 represent a mixed cluster with nuclear, ribosomal and cytosolic enriched terms such as cytosolic ribosome ($p < 10^{-40}$), nucleolus ($p < 10^{-30}$) and cytosolic part ($p < 10^{-25}$). The final phenotype is enriched for chromatin and chromosome ($p < 10^{-10}$) suggesting sub-nuclear resolution. Furthermore, as a result of quantifying uncertainty, we can see in figure 5 there are potentially more sub-cellular structures. However, the uncertainty is too great to support these phenotypes.

3.3.2 Mouse primary neuron cells (Itzhak et. al 2017)

The mouse neuron dataset reveals 10 phenotypes after we apply Novelty TAGM. However 8 of these phenotypes have no enriched GO annotations. This is likely a manifestation of the dispersed nature of this dataset, where the variability is generated by technical artefacts rather than biological signal. However, despite this Novelty TAGM is able to detect two relevant phenotypes: the first phenotype is enriched for nucleolus ($p < 0.01$); the second for chromosome ($p < 0.01$). This suggests additional annotations for this dataset.

3.3.3 HeLa cells (Hirst et. al 2018)

The HeLa dataset of Hirst *et al.* (2018), which we refer to HeLa Hirst, reveals 7 phenotypes with at least 1 protein with discovery probability greater than 0.95. However, three of these phenotypes represent singleton proteins. Phenotype 1 reveals a mixed cytosol/ribosomal annotations with the terms cytosolic ribosome ($p < 10^{-30}$) and cytosolic part ($p < 10^{-25}$) significantly over-represented. There are no further phenotypes enriched annotations (threshold $p = 0.01$), except phenotype 2 which is represents a mixed extracellular and cytosolic cluster. For example the terms extracellular organelle ($p < 10^{-13}$) and cytosol ($p < 10^{-10}$) are over-represented.

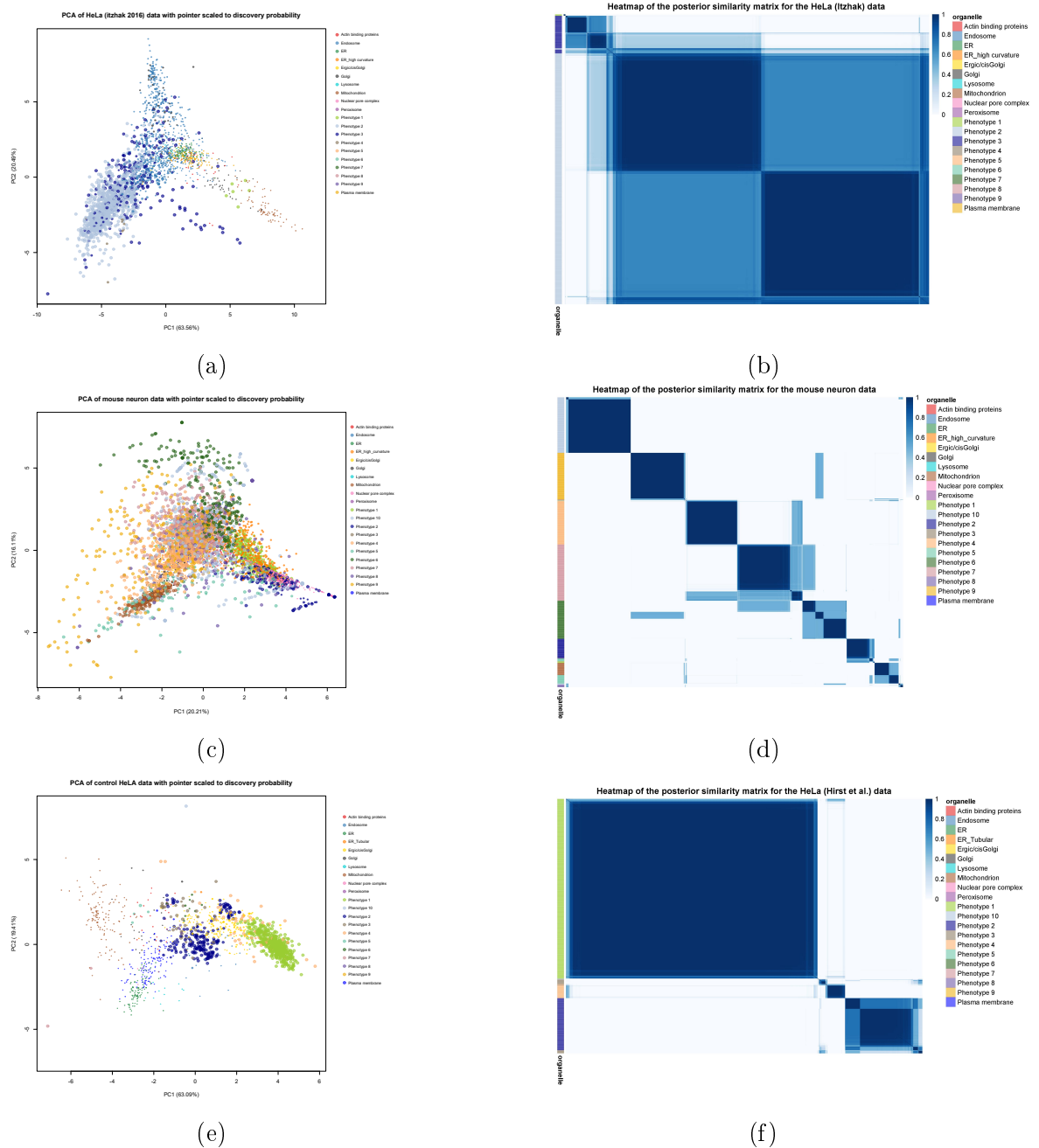


Figure 5: (a),(b),(c) PCA plots of the HeLa Itzhak data, mouse neuron data and HeLa Hirst data. The pointers are coloured according to the assigned organelle or phenotype and scaled according to their discovery probability. (d),(e),(f) Heatmaps of the HeLa Itzhak data, mouse neuron data and HeLa Hirst data. Only the proteins whos discovery probability is greater than 0.99 and outlier probability less than 0.95 (10^{-2} for the mouse neuron dataset to reduce number of visualised proteins) are shown. The heatmaps demonstrate the uncertainty in the clustering structure present in the data.

4 Comparison between Novelty TAGM and *phenoDisco*

In this section, we compare a already available novelty detection algorithm, *phenoDisco*, with Novelty TAGM. Despite both methods performing novelty detection the algorithms are quite distinct. The first major difference is that Novelty TAGM is a Bayesian method and as a result performs uncertainty quantification. Novelty TAGM quantifies the uncertainty in both the number of newly identified phenotypes and whether individual protein should belong to a new phenotypes. On other hand, *phenoDisco* must use the heuristic BIC to decide the number of phenotypes and does not provide an estimate of individual protein to phenotype allocation uncertainty. Another difference is the input to both methods, Novelty TAGM uses the data directly; *phenoDisco* takes the first two principal components as input. *Phenodisco* also requires an additional parameters - the minimum group size. This parameter can be challenging to specify, since there is a trade off between identifying functionally relevant phenotypes of different sizes and picking up small spurious protein clusters. Furthermore, *phenoDisco* struggles to scale to many of the datasets presented in this manuscript, because it requires iteratively refitting models and building of an outlier test statistic.

To demonstrate the difference between the two approaches we apply *phenoDisco* and Novelty TAGM to a spatial proteomics experiment on HEK-293 cells (Breckels *et al.*, 2013). PCA plots in figure 6 reveal broad similarities in the location of discovered phenotypes. Clearly, Novelty TAGM provides more information by scaling the pointer size to the discovery probability. We note that both methods reveal 8 phenotypes in the data, where for Novelty TAGM a phenotype needs at least one protein with discovery probability greater than 0.95. Figure 6 (panels d and e) reveal the distribution of proteins across these phenotypes. We conclude both approaches are able to discover small and large phenotypes without difficulty, with both methods identifying phenotypes with a few proteins, but also phenotypes with greater than 100 proteins. Figure 6 (panel f) show that both methods find the same number of phenotypes, however, not all of these phenotypes are functionally enriched. For *phenoDisco* 4 of the phenotypes had at least 1 significant Gene Ontology term, whereas this was true for 5 of the Novelty TAGM. Figure 6 (panel g) characterises the protein overlap between the two approaches. We see that both methods are in broad agreement, with most of the disagreement attributed when one method assigns a protein as unknown whilst the other allocate to a phenotype or organelle. A few notable disagreements occur, for example Novelty TAGM associates *phenoDisco* phenotype 3, which is a Lysosome enriched phenotype, to the PM. On the other hand, Novelty TAGM phenotypes 2 an 3, enriched for chromatin and ribosome respectively, are associated to the mitochondria by *phenoDisco*.

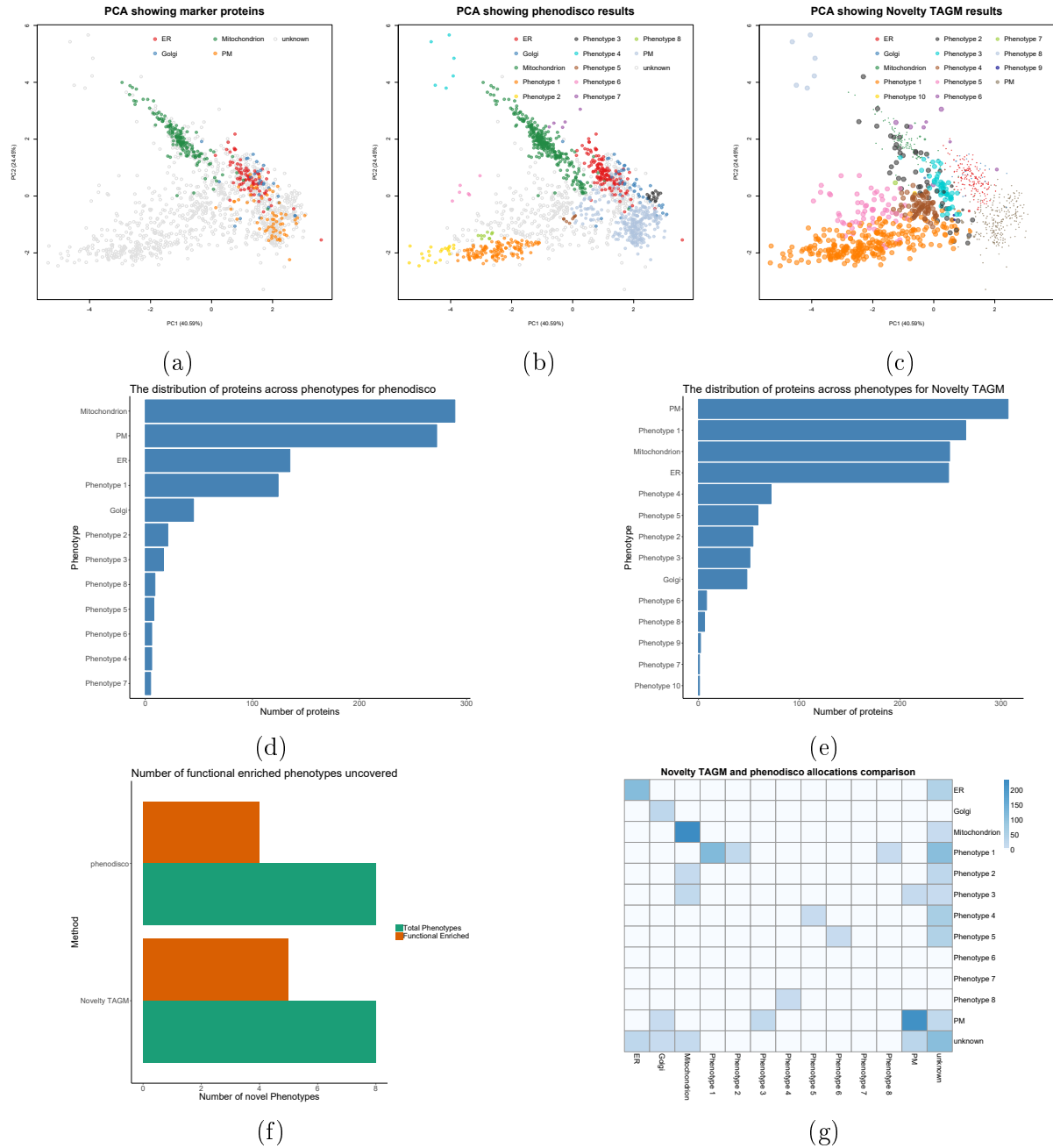


Figure 6: (a) PCA plot showing marker proteins for HEK data. (b) PCA plot with phenotypes identified by *phenoDisco*, (c) PCA plot with phenotypes identified by Novelty TAGM with pointer size scaled to discovery probability, (d, e) A barplots showing the number of proteins allocated to different phenotypes by *phenoDisco* and Novelty TAGM respectively. (f) A barplot demonstrating the proportion of phenotypes with functional enrichment for both methods. (g) A heatmap showing the overlap between *phenoDisco* and Novelty TAGM allocations.

5 Improved annotation allows exploration of endosomal processes

Given the information that the U 2-OS hyperLOPIT dataset resolves an endosomal cluster, we perform a re-analysis of this dataset focusing on the endosomes. We curate a set of marker proteins for the endosomes and add these annotations to the U 2-OS hyperLOPIT dataset. After which, we apply our Bayesian generative classifier TAGM to the data with this additional annotation (Crook *et al.*, 2018). Protein allocations to each subcellular niche can be visualised in the PCA plot of figure 7 (panel a). Figure 7 (panel b) demonstrates the increased number of protein that can be characterised by improved annotation of the U 2-OS cell line. Furthermore, we explore 8 proteins with uncertain endosomal localisation, which can be visualised in each of the violin plots in 7 (panel d), where available, we compare with HPA immuno-staining.

Q92738 (RN-tre) is an intracellular trafficking protein involved in retrograde transport from the endocytic pathway to the Golgi apparatus (Haas *et al.*, 2007). RN-tre acts on Rab5, as a GTPase activating protein and in complex with the Eps8, for EGF dependant receptor internalisation (Lanzetti *et al.*, 2000). Additionally, RN-tre targets Rab43 for the regulation of Shiga toxin by transporting it from the early endosome to the trans-golgi network (Fuchs *et al.*, 2007). Here we observe a steady-state snapshot of the localisations of RN-tre with potential localisation to the endosome and plasma membrane.

Q15833 (STXBP2) is a protein of interest because genetic mutations are linked with adverse patient outcome of familial hemophagocytic lymphohistiocytosis type 5 (FHL5) (zur Stadt *et al.*, 2009; Pagel *et al.*, 2012) and is required for platelet secretion (Al Hawas *et al.*, 2012). The biological function of STXBP2 is to regulate vesicle to membrane fusion by mediatation of the SNARE complex (Martin-Verdeaux *et al.*, 2003; Sigismund *et al.*, 2012). The endosomal/PM localisation of STXBP2 is thus inline with its biological role.

P61020 (RAB5B), a monomeric G protein, is a constituent member of the RAS oncogene superfamily. RAB5B binds directly to EEA1 via the N-terminus and the C-terminal domain of EEA1 binds to the endosome, constituting direct evidence for endosomal localisation (Callaghan *et al.*, 1999). This is supported by its HPA localisation to vesicles (figure 7 (panel b)) and so the endosomal localisation observed here is unsurprising.

O15498 (YKT6) is part of a SNARE complex which is involved with retrograde transport from the endosome to the Golgi apparatus (Tai *et al.*, 2004). We observed a mixed steady-state localisation of YKT6 between the cytosol and endosome. The cytosolic localisation is supported by the HPA annotation (figure 7 (panel b)) and endosomal localisation is further evidence of its role in vesicle docking in endocytosis.

Q9NZN3 (EHD3) is part of the EHD family of proteins that, through interaction with RAB11, regulate endocytic recycling (Naslavsky *et al.*, 2006; George *et al.*, 2007). HPA information (figure 7 (panel b)) and previous studies have also observed plasma membrane localisation (George *et al.*, 2007), suggesting a role for this protein in rapid recycling protein transport.

P20339 (RAB5A), a small GTPase and key regulator of membrane trafficking, forms a complex with the EEA1 C(2)H(2) zinc finger binding at the N-terminus (Mishra *et al.*, 2010) and thus associates RAB5A with the endosomal tethering. Potential localisation of

RAB5A to the early endosome (Fouraux *et al.*, 2004; Hunker *et al.*, 2006) and its role in endocytosis also permits the potential PM localisation observed here.

Q96L93 (KIF16B) is a highly dynamic kinesin-like plus end-directed microtubule-dependent motor protein involved in endosome transport and receptor recycling (Hoepfner *et al.*, 2005). Thus, a mixed localisation between endosome and PM is reflective of its biological roles, however HPA data clearly localises this protein to the Mitochondria (figure 7 (panel b)). This contradicts the supposed biological role of this protein, which arises from the uncertainty surrounding the uncertain specificity of the antibody (Thul *et al.*, 2017).

Q8NHG (ZNRF2), a E3 ubiquitin ligase, which is a substrate of mTOR and interacts with the mTORC1 complex (Hoxhaj *et al.*, 2016). Previous studies have suggested endosomal, lysosomal and membrane localisation for ZNRF2 (Araki and Milbrandt, 2003; Hoxhaj *et al.*, 2016). The localisation observed here is supportive of these previous studies.

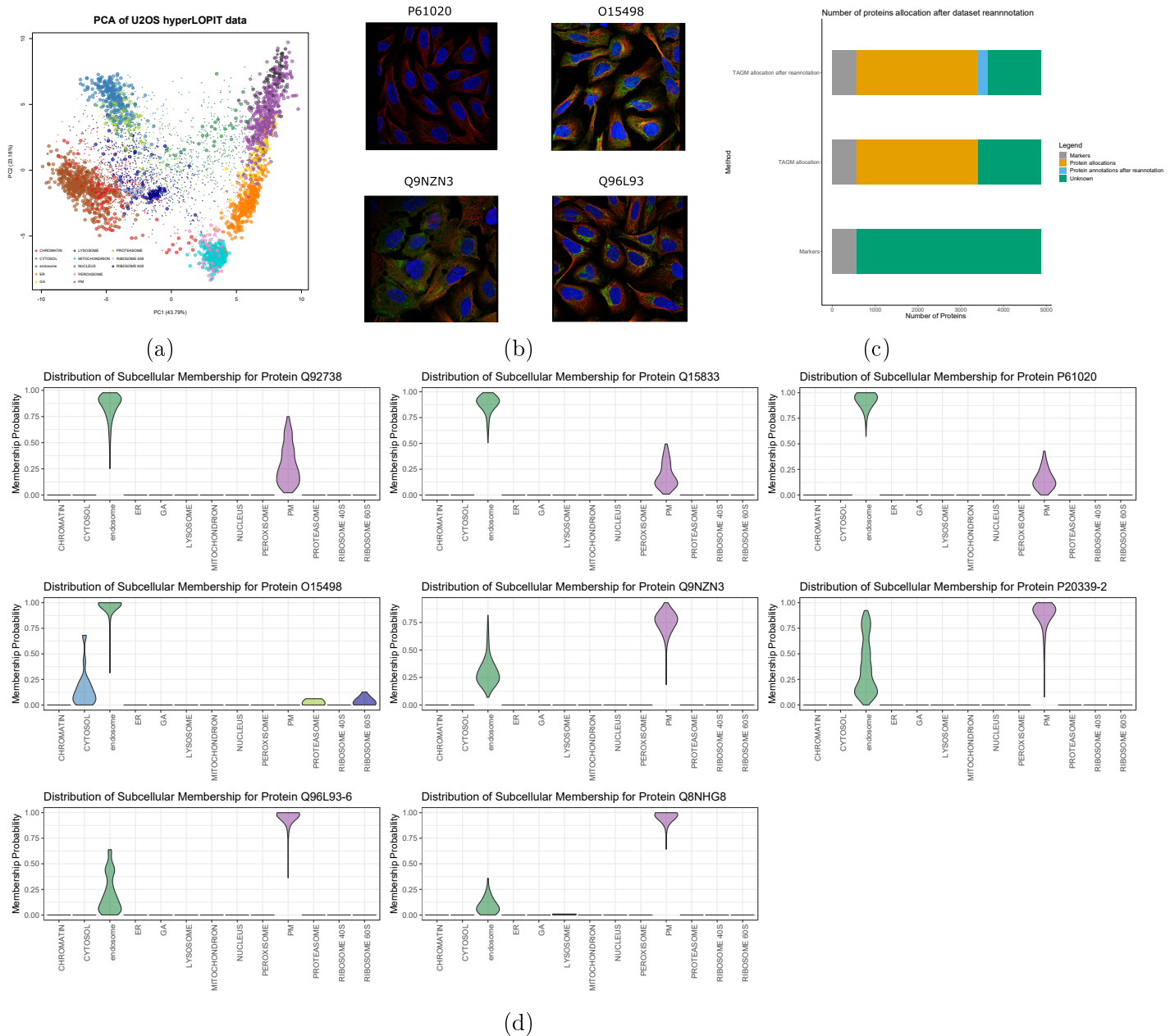


Figure 7: (a) PCA of hyperLOPIT data with pointer scaled to localisation probability and outliers shrunk. Points are coloured according to their post probable organelle. (b) Subcellular localisation of 4 proteins from HPA data using indirect immunofluorescence microscopy. The nucleus is stained in blue; microtubules in red, and the antibody staining targeting the protein in green. (c) A barplot representing the number of proteins allocated before and after re-annotation of the endosomal class (d) Violin plots of full probability distribution of proteins to organelles, where each violin plot is for a single protein.

6 Discussion

We have presented a semi-supervised Bayesian approach that simultaneously allows probabilistic allocation of proteins to organelles, detection of outlier proteins, as well as the discovery of novel sub-cellular structures. Our method unifies several approaches present in the literature, combining the ideas of supervised machine learning and unsupervised structure discovery. Formulating inference in a Bayesian framework allows for the quantification of uncertainty; in particular, the uncertainty in the number of newly discovered annotations.

Our proposed methodology allows us to interrogate individual proteins to see whether they belong to a newly discovered phenotype. Through the posterior similarity matrix we can visualise the global patterns in the uncertainty in phenotype discovery. We summarise this posterior similarity matrix into a single clustering by maximising the posterior expected adjusted rand index. This methodology infers the number of clusters supported by the data, rather than many ad-hoc approaches which require specification of the number of clusters.

Application of our method across 10 different spatial proteomics experiments with diverse protocols and varying levels of resolution revealed additional annotation in every single experiment. Our analysis recovered and validated chromatin enrichment preparation experimental design in *hyperLOPIT* datasets. Our approach also revealed additional sub-cellular niches in the mouse stem cell dataset and U 2-OS *hyperLOPIT* dataset.

Our method revealed resolution of 4 sub-nuclear compartments in the U 2-OS *hyperLOPIT* dataset, which was validated by human protein atlas annotations. An additional endosome-enriched phenotype was uncovered and Novelty TAGM robustly identified an overlapping phenotype in LOPIT-DC data providing strong evidence for endosomal resolution. Further biologically relevant annotations were uncovered in these datasets as well as other datasets. For example, a group of vesicle proteins involved in transport from the ER to the early Golgi was identified in the yeast dataset; resolution of the ribosomal subunit was identified in the fibroblast dataset, and separate nuclear, cytosolic and ribosomal annotations were identified in DOM datasets.

Thus our approach is widely applicable within the field of spatial proteomics and builds upon state-of-the-art approaches. The computational algorithms presented here are disseminated as part of the Bioconductor project ([Gentleman *et al.*, 2004](#); [Huber *et al.*, 2015](#)) building on MS-based data structures provided in [Gatto and Lilley \(2012\)](#) and are disseminated as part of the pRoloc suite, with all data provided in pRolocdata ([Gatto *et al.*, 2014b](#)).

During our analysis, we observed that the posterior similarity matrices have potential sub-clustering structures. Many known organelles and sub-cellular niches have sub-compartmentalisation, thus methodology to detect sub-compartmentalisation is in preparation. Furthermore, we have observed that different experiments and different data modalities share information. Integrative approaches to spatial proteomics analysis are also desired.

7 Appendix

7.1 Handling label switching

Bayesian inference in mixture models suffers from an identifiability issue known as *label switching* - a phenomenon where the allocation labels can flip between runs of the algorithm (Richardson and Green, 1997; Stephens, 2000). This occurs because of the symmetry of the likelihood function under permutations of these labels. We note that this only occurs in unsupervised or semi-supervised mixture models. This makes inference of the parameters in mixture models challenging. In our setting the labels for the known components do not switch, but for the new phenotypes label switching must occur. One standard approach to circumvent this issue is to form the so-called *posterior similarity matrix* (PSM) (Fritsch and Ickstadt, 2009). The PSM is an $N \times N$ matrix where the $(i, j)^{th}$ entry is the posterior probability that protein i and protein j reside in the same component. More precisely, if we let S denote the PSM and T denote the number of Monte-Carlo iterations then

$$S_{ij} = P(z_i = z_j | X, \boldsymbol{\theta}, \boldsymbol{\pi}, \kappa, \epsilon, \mathbf{M}, V) \approx \frac{1}{T} \sum_{t=1}^T \mathbb{I}(z_i^{(t)} = z_j^{(t)}), \quad (8)$$

where \mathbb{I} denotes the indicator function. The PSM is clearly invariant to label switching and so avoids the issues arising from the *label switching* problem.

7.2 Summarising posterior similarity matrices

To summarise the PSMs, we take the approach proposed by Fritsch and Ickstadt (2009). They proposed the adjusted Rand index (AR) (Rand, 1971; Hubert and Arabie, 1985), a measure of cluster similarity, as a utility function and then we wish to find the allocation vector \hat{z} that maximises the expected adjusted Rand index with respect to the true clustering z . Formally, we write

$$\hat{z} = \arg \max_{z^*} E[AR(z^*, z) | X, \boldsymbol{\theta}, \boldsymbol{\pi}, \kappa, \epsilon, \mathbf{M}, V], \quad (9)$$

which is known as the Posterior Expected Adjusted Rand index (PEAR). One obvious pitfall is that this quantity depends on the unknown true clustering z . However, this can be approximated from the MCMC samples:

$$PEAR \approx \frac{1}{T} \sum_{t=1}^T AR(z^*, z^{(t)}). \quad (10)$$

The space of all possible clustering over which to maximise is infeasibly large to explore. Thus we take an approach taken in Fritsch and Ickstadt (2009) to propose candidate clusterings over which to maximise. Using hierarchical clustering with distance $1 - S_{ij}$, the PEAR criterion is computed for clusterings at every level of the hierarchy. The optimal clustering \hat{z} is the allocation vector which maximises the PEAR.

7.3 Details of MCMC

The MCMC algorithm used in [Crook *et al.* \(2018\)](#) is insufficient to handle inference of unknown phenotypes. A collapsed Gibbs sampler approach is used, but a number of modifications are made. Firstly, to accelerate convergence of the algorithm half the proteins are initially allocated randomly amongst the new phenotypes. Secondly, the parameters for the new phenotypes are proposed from the prior. Throughout the same default prior choices are used as in [Crook *et al.* \(2018\)](#).

References

- Al Hawas, R. et al. (2012). Munc18b/stxbp2 is required for platelet secretion. *Blood*, **120**(12), 2493–2500.
- Antoniak, C. E. (1974). Mixtures of dirichlet processes with applications to bayesian non-parametric problems. *Ann. Statist.*, **2**(6), 1152–1174.
- Araki, T. et al. (2003). Znrf proteins constitute a family of presynaptic e3 ubiquitin ligases. *Journal of Neuroscience*, **23**(28), 9385–9394.
- Ashburner, M. et al. (2000). Gene ontology: tool for the unification of biology. *Nature genetics*, **25**(1), 25–29.
- Beltran, P. M. J. et al. (2016). A portrait of the human organelle proteome in space and time during cytomegalovirus infection. *Cell systems*, **3**(4), 361–373.
- Benjamini, Y. et al. (1995). Controlling the false discovery rate: a practical and powerful approach to multiple testing. *Journal of the royal statistical society. Series B (Methodological)*, pages 289–300.
- Breckels, L. M. et al. (2013). The effect of organelle discovery upon sub-cellular protein localisation. *Journal of proteomics*, **88**, 129–140.
- Breckels, L. M. et al. (2016). Learning from heterogeneous data sources: an application in spatial proteomics. *PLoS computational biology*, **12**(5), e1004920.
- Bue, C. A. et al. (2006). Erv26p directs pro-alkaline phosphatase into endoplasmic reticulum-derived coat protein complex ii transport vesicles. *Molecular biology of the cell*, **17**(11), 4780–4789.
- Callaghan, J. et al. (1999). Direct interaction of eea1 with rab5b. *European journal of biochemistry*, **265**(1), 361–366.
- Cappellaro, C. et al. (1998). New potential cell wall glucanases of *Saccharomyces cerevisiae* and their involvement in mating. *Journal of bacteriology*, **180**(19), 5030–5037.
- Christoforou, A. et al. (2016). A draft map of the mouse pluripotent stem cell spatial proteome. *Nature communications*, **7**, 9992.
- Crook, O. M. et al. (2018). A bayesian mixture modelling approach for spatial proteomics. *PLOS Computational Biology*, **14**(11), 1–29.
- Delic, M. et al. (2013). The secretory pathway: exploring yeast diversity. *FEMS microbiology reviews*, **37**(6), 872–914.
- Dunkley, T. P. et al. (2004). Localization of organelle proteins by isotope tagging (lopit). *Molecular & Cellular Proteomics*, **3**(11), 1128–1134.

- Dunkley, T. P. et al. (2006). Mapping the arabidopsis organelle proteome. *Proceedings of the National Academy of Sciences*, **103**(17), 6518–6523.
- Ferguson, T. S. (1974). Prior distributions on spaces of probability measures. *Ann. Statist.*, **2**(4), 615–629.
- Foster, L. J. et al. (2006). A mammalian organelle map by protein correlation profiling. *Cell*, **125**(1), 187–199.
- Fouraux, M. A. et al. (2004). Rabip4' is an effector of rab5 and rab4 and regulates transport through early endosomes. *Molecular biology of the cell*, **15**(2), 611–624.
- Fritsch, A. et al. (2009). Improved criteria for clustering based on the posterior similarity matrix. *Bayesian Anal.*, **4**(2), 367–391.
- Fuchs, E. et al. (2007). Specific rab gtpase-activating proteins define the shiga toxin and epidermal growth factor uptake pathways. *The Journal of cell biology*, **177**(6), 1133–1143.
- Gatto, L. et al. (2012). Msbase - an r/bioconductor package for isobaric tagged mass spectrometry data visualization, processing and quantitation. *Bioinformatics*, **28**, 288–289.
- Gatto, L. et al. (2010). Organelle proteomics experimental designs and analysis. *Proteomics*, **10**(22), 3957–3969.
- Gatto, L. et al. (2014a). A foundation for reliable spatial proteomics data analysis. *Molecular & Cellular Proteomics*, pages mcp–M113.
- Gatto, L. et al. (2014b). Mass-spectrometry based spatial proteomics data analysis using proloc and prolocredata. *Bioinformatics*.
- Gatto, L. et al. (2018). Assessing sub-cellular resolution in spatial proteomics experiments. *bioRxiv*.
- Geladaki, A. et al. (2019). Combining loipit with differential ultracentrifugation for high-resolution spatial proteomics. *Nature Communications*, **10**, 331.
- Gentleman, R. C. et al. (2004). Bioconductor: open software development for computational biology and bioinformatics. *Genome biology*, **5**(10), R80.
- George, M. et al. (2007). Shared as well as distinct roles of ehd proteins revealed by biochemical and functional comparisons in mammalian cells and c. elegans. *BMC cell biology*, **8**(1), 3.
- Gibson, T. J. (2009). Cell regulation: determined to signal discrete cooperation. *Trends in biochemical sciences*, **34**(10), 471–482.
- Groen, A. J. et al. (2014). Identification of trans-golgi network proteins in arabidopsis thaliana root tissue. *Journal of proteome research*, **13**(2), 763–776.

- Haas, A. K. et al. (2007). Analysis of gtpase-activating proteins: Rab1 and rab43 are key rabs required to maintain a functional golgi complex in human cells. *Journal of cell science*, **120**(17), 2997–3010.
- Hirst, J. et al. (2018). Role of the ap-5 adaptor protein complex in late endosome-to-golgi retrieval. *PLoS biology*, **16**(1), e2004411.
- Hoepfner, S. et al. (2005). Modulation of receptor recycling and degradation by the endosomal kinesin kif16b. *Cell*, **121**(3), 437–450.
- Hoxhaj, G. et al. (2016). The e3 ubiquitin ligase znrfl2 is a substrate of mtorc1 and regulates its activation by amino acids. *elife*, **5**, e12278.
- Huber, W. et al. (2015). Orchestrating high-throughput genomic analysis with bioconductor. *Nature methods*, **12**(2), 115–121.
- Hubert, L. et al. (1985). Comparing partitions. *Journal of Classification*, **2**(1), 193–218.
- Huh, W.-K. et al. (2003). Global analysis of protein localization in budding yeast. *Nature*, **425**(6959), 686.
- Hunker, C. et al. (2006). Rab5-activating protein 6, a novel endosomal protein with a role in endocytosis. *Biochemical and biophysical research communications*, **340**(3), 967–975.
- Inadome, H. et al. (2005). Immunoisolation of the yeast golgi subcompartments and characterization of a novel membrane protein, svp26, discovered in the sed5-containing compartments. *Molecular and cellular biology*, **25**(17), 7696–7710.
- Itzhak, D. N. et al. (2016). Global, quantitative and dynamic mapping of protein subcellular localization. *Elife*, **5**, e16950.
- Itzhak, D. N. et al. (2017). A mass spectrometry-based approach for mapping protein subcellular localization reveals the spatial proteome of mouse primary neurons. *Cell reports*, **20**(11), 2706–2718.
- Kau, T. R. et al. (2004). Nuclear transport and cancer: from mechanism to intervention. *Nature Reviews Cancer*, **4**(2), 106–117.
- Kirk, P. et al. (2012). Bayesian correlated clustering to integrate multiple datasets. *Bioinformatics*, **28**(24), 3290–3297.
- Kristensen, A. R. et al. (2014). Protein correlation profiling-silac to study protein-protein interactions. In *Stable Isotope Labeling by Amino Acids in Cell Culture (SILAC)*, pages 263–270. Springer.
- Kristensen, A. R. et al. (2012). A high-throughput approach for measuring temporal changes in the interactome. *Nature methods*, **9**(9), 907.
- Lanzetti, L. et al. (2000). The eps8 protein coordinates egf receptor signalling through rac and trafficking through rab5. *Nature*, **408**(6810), 374.

- Laurila, K. et al. (2009). Prediction of disease-related mutations affecting protein localization. *BMC genomics*, **10**(1), 122.
- Martin-Verdeaux, S. et al. (2003). Evidence of a role for munc18-2 and microtubules in mast cell granule exocytosis. *Journal of cell science*, **116**(2), 325–334.
- McAlister, G. C. et al. (2014). Multinotch ms3 enables accurate, sensitive, and multiplexed detection of differential expression across cancer cell line proteomes. *Analytical chemistry*, **86**(14), 7150–7158.
- Mishra, A. et al. (2010). Structural basis for rab gtpase recognition and endosome tethering by the c2h2 zinc finger of early endosomal autoantigen 1 (eea1). *Proceedings of the National Academy of Sciences*, **107**(24), 10866–10871.
- Mulvey, C. M. et al. (2017). Using hyperLOPIT to perform high-resolution mapping of the spatial proteome. *Nature Protocols*, **12**(6), 1110–1135.
- Naslavsky, N. et al. (2006). Interactions between ehd proteins and rab11-fip2: a role for ehd3 in early endosomal transport. *Molecular biology of the cell*, **17**(1), 163–177.
- Nightingale, D. J. H. et al. (2019). The subcellular organisation of saccharomyces cerevisiae. *Current Opinion in Chemical Biology*, **48**(11), 1–10.
- Orre, L. M. et al. (2019). Subcellbarcode: Proteome-wide mapping of protein localization and relocalization. *Molecular Cell*, **73**(1), 166 – 182.e7.
- Otte, S. et al. (2001). Erv41p and erv46p: new components of copii vesicles involved in transport between the er and golgi complex. *The Journal of cell biology*, **152**(3), 503–518.
- Pagel, J. et al. (2012). Distinct mutations in stxbp2 are associated with variable clinical presentations in patients with familial hemophagocytic lymphohistiocytosis type 5 (fhl5). *Blood*, **119**(25), 6016–6024.
- Pardo, M. et al. (2004). Pst1 and ecm33 encode two yeast cell surface gpi proteins important for cell wall integrity. *Microbiology*, **150**(12), 4157–4170.
- Rand, W. M. (1971). Objective criteria for the evaluation of clustering methods. *Journal of the American Statistical association*, **66**(336), 846–850.
- Richardson, S. et al. (1997). On bayesian analysis of mixtures with an unknown number of components (with discussion). *Journal of the Royal Statistical Society: series B (statistical methodology)*, **59**(4), 731–792.
- Rousseau, J. et al. (2011). Asymptotic behaviour of the posterior distribution in overfitted mixture models. *Journal of the Royal Statistical Society: Series B (Statistical Methodology)*, **73**(5), 689–710.
- Schwarz, G. et al. (1978). Estimating the dimension of a model. *The annals of statistics*, **6**(2), 461–464.

- Sigismund, S. et al. (2012). Endocytosis and signaling: cell logistics shape the eukaryotic cell plan. *Physiological reviews*, **92**(1), 273–366.
- Siljee, J. E. et al. (2018). Subcellular localization of MC4R with ADCY3 at neuronal primary cilia underlies a common pathway for genetic predisposition to obesity. *Nat Genet*.
- Stephens, M. (2000). Dealing with label switching in mixture models. *Journal of the Royal Statistical Society: Series B (Statistical Methodology)*, **62**(4), 795–809.
- Sullivan, D. P. et al. (2018). Deep learning is combined with massive-scale citizen science to improve large-scale image classification. *Nature biotechnology*, **36**(9), 820.
- Tai, G. et al. (2004). Participation of the syntaxin 5/ykt6/gs28/gs15 snare complex in transport from the early/recycling endosome to the trans-golgi network. *Molecular biology of the cell*, **15**(9), 4011–4022.
- Tan, D. J. et al. (2009). Mapping organelle proteins and protein complexes in drosophila melanogaster. *Journal of proteome research*, **8**(6), 2667–2678.
- Thompson, A. et al. (2003). Tandem mass tags: a novel quantification strategy for comparative analysis of complex protein mixtures by ms/ms. *Analytical chemistry*, **75**(8), 1895–1904.
- Thul, P. J. et al. (2017). A subcellular map of the human proteome. *Science*, **356**(6340), eaal3321.
- Ting, L. et al. (2011). Ms3 eliminates ratio distortion in isobaric multiplexed quantitative proteomics. *Nature methods*, **8**(11), 937.
- Wendler, F. et al. (2010). A genome-wide rna interference screen identifies two novel components of the metazoan secretory pathway. *The EMBO journal*, **29**(2), 304–314.
- Yin, Q. Y. et al. (2005). Comprehensive proteomic analysis of saccharomyces cerevisiae cell walls identification of proteins covalently attached via glycosylphosphatidylinositol remnants or mild alkali-sensitive linkages. *Journal of Biological Chemistry*, **280**(21), 20894–20901.
- Yofe, I. et al. (2016). One library to make them all: streamlining the creation of yeast libraries via a swap-tag strategy. *Nature methods*, **13**(4), 371.
- Yu, G. et al. (2012). clusterProfiler: an R package for comparing biological themes among gene clusters. *Omics: a journal of integrative biology*, **16**(5), 284–287.
- zur Stadt, U. et al. (2009). Familial hemophagocytic lymphohistiocytosis type 5 (fhl-5) is caused by mutations in munc18-2 and impaired binding to syntaxin 11. *The American Journal of Human Genetics*, **85**(4), 482–492.